Absorption coefficient of urban aerosol in Nanjing, west Yangtze River Delta of China

B. L. Zhuang[1, 4, *], T. J. Wang[1, 4], J. Liu[1,2], Y. Ma[3], C. Q. Yin[1], S. Li[1, 4], M. Xie[1, 4], Y. Han[1, 4], J. L. Zhu[1], X. Q. Yang[1, 4], C. B. Fu[1, 4]

[1] School of Atmospheric Sciences, Nanjing University, Xianlin Ave. 163, Nanjing 210023, China

[2] University of Toronto, Toronto M5S 3G3, Canada

[3] School of Environmental Science and Engineering, Nanjing University of Information Science and Technology, Ningliu Rd. 219, Nanjing 210044, China

[4] Collaborative Innovation Center of Climate Change, Jiangsu Province, China

[*] Corresponding author, E-mail: blzhuang@nju.edu.cn; Tel.: +862589681156; fax: +862589683797

Abstract: Absorbing aerosols can significantly modulate shortwave solar radiation in the atmosphere, affecting regional and global climate. Aerosol absorption coefficient (AAC) is an indicator to assess the impact of absorbing aerosols on radiative forcing. In this study, the near-surface AAC and absorption angstrom exponent (AAE) in urban Nanjing, China, are characterized on the basis of measurements in 2012 and 2013 using the 7-channel Aethalometer (model AE-31, Magee Scientific, USA). The AAC is estimated with direct and indirect corrections, which show consistent temporal variations and magnitudes of AAC at 532 nm. The mean AAC at 532 nm is about 43.23±28.13 Mm^{-1} in urban Nanjing, which is much lower than that in Pearl River Delta and as the same as that in rural areas (Lin'an) in Yangtze River Delta. The AAC in urban Nanjing shows strong seasonality (diurnal variations), high in cold seasons (at rush hours) and low in summer (in afternoon). It also show synoptic and quasi-two-week cycles in response to weather systems. Its frequency distribution follows a typical lognormal pattern. The 532 nm-AAC ranging from 15 to 65 Mm^{-1} dominates, accounting for more than 72% of the total data samples in the entire study period. Frequent high pollution episodes, such as those

observed in June 2012 and in winter 2013, greatly enhanced AAC and altered its temporal variations and frequency distributions. These episodes are mostly due to local emissions and regional pollutions. Air masses from northern China to Nanjing can sometimes be highly polluted and lead to high AAC at the site. AAE at 660/470 nm from the Schmid correction (Schmid et al., 2006) is about 1.56, which might be more reasonable compared to that from the Weingartner correction (Weingartner et al., 2003). Low AAEs mainly appear in summer in response to the relative humidity (RH). AAC increases with increasing AAE at a fixed aerosol loading. The RH-AAC relationship is more complex. Overall, AAC peaks around RH values of 40% (1.3<AAE<1.6), 65% (AAE<1.3 and AAE>1.6), and 80% (1.3<AAE<1.6).

1 Introduction

Atmospheric aerosols, their loadings having increased in recent years, can significant influence regional or global climate because of their direct and indirect interactions with shortwave solar radiation in the atmosphere (Forster et al., 2007). Absorbing aerosols, which is mostly composed of dust in desert areas and of black carbon (BC) in the regions with frequent human activities, can strongly absorb solar radiation, resulting in changes in the atmospheric circulations and hydrological cycle. Although the warming effect of CO_2 could be greatly offset by the scattering aerosol direct effect in the regions with high aerosol concentrations (Kiehl and Briegleb, 1993), it might be further strengthened by BC aerosols because the warming effect of BC aerosols on the global scale is significant, only surpassed by CO_2 (Jacobson 2002). Menon et al. (2002) suggested that the trend of precipitation in China over the past decades, with increased rainfall in the south and drought in the north, might be related to the variation of BC in the region.

47 Previous studies have focused on the aerosol optical properties, radiative forcing and climate
48 effects in both global and regional scales, from model simulations (Penner et al., 2001; Liao and
49 Seinfeld, 2005; Zhuang et al., 2013a; b) and satellite/ground-based observations (Bellouin et al., 2003;
50 Yan et al., 2008; Wu et al., 2012; Zhuang et al., 2014a; etc.) in the past 20 years. Forster et al. (2007)
51 simulated the global mean direct radiative forcing of total aerosols and BC, which ranges between
52 +0.04 and -0.63 W m^{-2} and between +0.1 and +0.3 W m^{-2}, respectively. Over East Asia, the simulated
53 BC direct raidative forcing varies from +0.32 to +0.81 W m^2 (Zhuang et al., 2013a). All above showed
54 significant uncertainties in estimating the aerosol direct radiative forcing in numerical models. These
55 uncertainties were mostly due to the uncertainties in the aerosol optical properties (Holler et al., 2003)
56 which were related to the aerosol emissions, profiles, compositions and mixing states. Forster et al.
57 (2007) stated that the uncertainties could be reduced if observed aerosol optical properties were
58 employed when estimating the forcing. China has experienced rapid population and economic growth
59 during the past three decades, resulting in enhanced aerosol and trace gas emissions. Streets et al. (2001)
60 suggested that the BC emissions in China roughly accounts for one-fourth of the global anthropogenic
61 emissions, although the uncertainty about this estimate is large. The BC aerosols are mostly emitted in
62 Southwest, North China, Yangtze River Delta (YRD) and Pearl River Delta (PRD) regions (Zhang et al.,
63 2009). Recently, many observation-based studies are conducted on the aerosol optical properties and
64 direct radiative forcing over China (Xu et al., 2004; Yan, 2006; Xia et al., 2007; Yan et al., 2008; He et
65 al., 2009; Wang et al., 2009; Wu et al., 2009; Li et al., 2010; Cai et al., 2011; Bai et al., 2011; Xiao et al.,
66 2011; Zhou et al., 2011; Wu et al., 2012; etc.). Some of them focused on the total extinction or optical
67 depth of the aerosols. Xia et al. (2007) reported that the annual mean optical depth (AOD) at 500 nm
68 and Angstrom exponent (AE) of total aerosols in YRD were 0.77 and 1.17, respectively. Xiao et al.

(2011) analyzed the temporal and spatial variations of the total aerosol optical depth and Angstrom exponent using CE-318 in Hangzhou. Zhuang et al. (2014a) suggested that column AOD and AE of absorbing aerosols were 0.04±0.02 and 1.44±0.50 in urban Nanjing. The aerosol absorption coefficients (AAC) were also studied for several urban and rural areas of China. AAC at 565 nm in Gobi desert was found to be as low as 6 ± 11 Mm^{-1} (Yulin) (Xu et al. 2004). The annual 532 nm-AAC was about 17.54 ± 13.44 Mm^{-1} at a rural site while it was about 45 ± 39 Mm^{-1} at an urban site, in Beijing (Yan et al. 2008; He et al. 2009). AAC at 532 nm was as large as 82 ± 23 Mm^{-1} at urban areas of Pearl River Delta (PRD) in South China (Wu et al. 2009).

Although considerable researches on this issue have been performed, it's still insufficient in regional scale in China and there is a lack of study on AAC in YRD, one of the fastest growing regions in China. Therefore, this study is to address this issue by characterizing AAC in the region using the near-surface absorption coefficient and Angstrom exponent of absorbing aerosols in urban Nanjing, a typical developing city in west Yangtze River Delta of China. The method is described in Section 2. Results and discussions are presented in Section 3, followed by Conclusions in Section 4.

2 Methodologies

2.1 Sampling station and instruments

Sampling site is located in the Gulou campus of Nanjing University, urban Nanjing (32.05^{o} N, 118.78^{o} E). It is built on the roof of a 79.3 m-tall building, around which there are no industrial pollution sources within a 30 km radius but there are several main roads with apparent traffic pollution. The sketch map of the site (not shown) can be referred to Figure 1 of Zhu et al. (2012). The black carbon aerosol mass concentration and aerosol absorption coefficient were derived from the

measurements using the 7-channel Aethalometer (model AE-31, Magee Scientific, USA). The AE-31 model measures light attenuation at seven wavelengths (370, 470, 520, 590, 660, 880, and 950 nm, respectively). The aerosol inlet is located ~1 m above the roof. Routine flow calibration and blank tests were performed before sampling. Details on the AE-31 and its sampling principles can be referred to Hansen et al. (1984), Weingartner et al. (2003) and Arnott et al. (2005). Near-real-time continuous measurements were made at the site since 1 January 2012, using the AE-31, with a desired flow rate of 5.0 L/min and a sampling interval of 5 min. Two-year's data in 2012 and 2013 are used in this study. Meteorological data are from the National Meteorological Station of Nanjing (No. 58238).

2.2 Calculation of AE-31_absorption coefficient

The absorption coefficient is defined with Beer-Lambert's law as shown in Eq. 1 in Weingartner et al. (2003) and Arnott et al. (2005), which is associated with the intensities of the incoming light and remaining light after passing through a medium. A variable ATN, which is given as percentage value, is defined to represent filter attenuation through the sample spot in the tape (Eq. 2 in Weingartner et al., 2003 and Arnott et al., 2005) inside the instrument. Aerosol light absorption coefficient and BC mass concentration can be calculated directly based on the measured light attenuation through a quartz filter matrix. There are two ways in calculating aerosol light absorption coefficient. The indirect calculation (IDC for short), which is much simpler than the direct ones, is expressed as Eq. 1.

$$\sigma_{\mathrm{abs},t}(\lambda) = [BC] \times \gamma \quad (1)$$

where, [BC] is the mass concentration of Aethalometer BC (in μg/m^3) without any correction and γ is the conversion factor determined empirically from linear regression of the Aethalometer BC

concentration versus the aerosol absorption measurement (Yan et al., 2008). Wu et al. (2009) indicated that the conversion factor γ from the linear regression of the Aethalometer BC concentrations (ng/m^3) at 880 nm against the light absorption coefficient (Mm^{-1}) at 532 nm in South China was about 8.28 m^2/g. γ=11.05 m^2/g in the suburb of Nanjing.

In addition to the indirect way, wavelength-depended aerosol absorption coefficient can be calculated directly based on the measured light attenuation (ATN) at seven wavelengths (370, 440, 520, 590, 660, 880 and 950 nm) as shown in Eq. 2:

$$\sigma_{\mathrm{ATN},t}(\lambda)=\frac{(\mathrm{ATN}_t(\lambda)-\mathrm{ATN}_{t-1}(\lambda))}{\Delta t}\times\frac{A}{V} \quad (2)$$

where, A (in m^2) is the area of the aerosol-laden filter spot, V is the volumetric sampling flow rate (in L/min) and Δt is the time interval (=5 min) between t and $t-1$. It is well known that σ_{ATN} is generally larger than the actual aerosol absorption coefficient σ_{abs} because of the optical interactions of the filter substrate with the deposited aerosol (Petzold et al., 1997; Weingartner et al., 2003; Arnott et al., 2005; Schmid et al., 2006). The key factors leading to the bias include: 1) multiple scattering of light at the filter fibers (multiple scattering effect), which may result in the overestimation of the σ, and 2) instrumental response with increased particle loading on the filter (shadowing effect), which may lead to underestimation of the σ. Therefore, the calibration factors *C* and *R* (shown in Eq. 3) are introduced to address the scattering effect and shadowing effect, respectively:

$$\sigma_{\mathrm{abs},t}(\lambda)=\frac{\sigma_{\mathrm{ATN},t}(\lambda)}{C\times R} \quad (3)$$

To address the uncertainties, several correction algorithms, including Weingartner (Weingartner et al., 2003), Arnott (Arnott et al., 2005), Schmid (Schmid et al., 2006), Virkkula (Virkkula et al., 2007) corrections, have been developed. Collaud Coen et al. (2010) suggested that both Weingartner (WC2003 for short, hereinafter) and Schmid (SC2006 for short, hereinafter) corrected-absorptions have

good agreements with the one from Multi-Angle Absorption Photometer. Therefore, these two corrections, which have similar formula shown in Eq. 4, are applied in this study to investigate the absorption coefficient:

$$\sigma_{\mathrm{abs},t}(\lambda)=\frac{\sigma_{\mathrm{ATN},t}(\lambda)}{C\times((\frac{1}{f}-1)\times\frac{\ln(\mathrm{ATN}_t(\lambda))-\ln 10}{\ln 50-\ln 10}+1)} \tag{4}$$

Both of them have the same $R(\lambda)$:

$$R_t(\lambda)=(\frac{1}{f}-1)\times\frac{\ln(\mathrm{ATN}_t(\lambda))-\ln 10}{\ln 50-\ln 10}+1 \tag{5}$$

And R =1 when $\mathrm{ATN}\le 10$. f can be calculated according to Weingartner et al. (2003):

$$f(\lambda)=n\times(1-\omega(\lambda))+1 \tag{6}$$

Where ω is the wavelength depended single scattering albedo (SSA) and n is a constant (=0.86 ± 0.01). Note that the reliability of n value (0.86) is limited because this value is mostly estimated under the condition of $\omega<0.6$, which may result in large bias. Therefore, an empirical f =1.2 (when $\omega\simeq 0.9$), which is independent of wavelength as suggested by Schmid et al. (2006), is used for both WC2003 and SC2006 in this study.

The multiple-scattering correction in WC2003 is also different from that in SC2006. Weingartner (Weingartner et al., 2003) indicated that the two waveband (450 and 660 nm) averaged C was about 3.6 for non-fresh soot. In this study, C in WC2003 is independent of wavelength and is set 3.48 for China according to Wu et al. (2013). In contrast, Schmid (Schmid et al., 2006) pointed out that C, which is wavelength depended, is initially expressed as following:

$$C(\lambda)=C^{*}(\lambda)+m_s(\lambda)\times\frac{\omega(\lambda)}{1-\omega(\lambda)} \tag{7}$$

where m_s represents the fraction of the aerosol scattering coefficient and ω is SSA. Optical

properties from CE-318 were used in this study because there was no concomitant scattering measurements at the site during the whole sampling period. Thus, we assumed that SSA and Angstrom exponent (AE) at the low layers of atmosphere were equated to the column ones. According to Zhuang et al. (2014a), annual mean $\omega(440)$=0.922, $\omega(675)$=0.924, and $\alpha_{a,675/440nm}$=1.44 at the site. Based on $\alpha_{a,675/440nm}$ and according to the definition:

$$\omega(\lambda)=\frac{\sigma_s(\lambda)}{\sigma_s(\lambda)+\sigma_a(\lambda)} \tag{8}$$

$\alpha_{s,675/440nm}$ can be calculated as the following (Angstrom. 1929):

$$\alpha_{s,675/440nm}=-\frac{\log(\frac{\sigma_s(675)}{\sigma_s(440)})}{\log(675/440)}=-\frac{\log(\frac{1-\omega(440)}{\omega(440)}\times\frac{\omega(675)}{1-\omega(675)})}{\log(675/440)}+\alpha_{a,675/440nm} \tag{9}$$

Thus, $\alpha_{s,675/440nm}$=1.51.

All wavelength-depend SSAs could be calculated based on the following formula (Schmid et al., 2006):

$$\omega(\lambda)=\frac{\omega_0\times(\frac{\lambda}{\lambda_0})^{-\alpha_s}}{\omega_0\times(\frac{\lambda}{\lambda_0})^{-\alpha_s}+(1-\omega_0)\times(\frac{\lambda}{\lambda_0})^{-\alpha_a}} \tag{10}$$

Here, ω_0, λ_0, and $\alpha_{s,675/440}$ were set to 0.922, 440 nm and 1.51, respectively. Based on the given $C^*(\lambda)$ and $m_s(\lambda)$ in Table 1 of Arnott et al. (2005), $C(\lambda)$ of pure candle light soot was estimated. To parameterize the dependence among $C(\lambda)$, λ and α_a, $\ln(C)$ versus $\ln(\lambda)$ for α_a=1, 1.5, 2 and 2.5 were plotted in Figure 1 and a quadratic fit (universal formula as shown in Eq. 11) for each α_a value was made following Schmid (Schmid et al., 2006) who suggested that the fits in Figure 1 were applicable to other kind of soot based on given ω and α_s.

$$\ln(C(\lambda))=A\times\ln(\lambda)^2+B\times\ln(\lambda)+D \tag{11}$$

174 Eq. 11 can be transformed into:

175 $$C(\lambda) = C_{ref} \times \frac{\lambda^{A\times\ln(\lambda)+B}}{\lambda_{ref}^{A\times\ln(\lambda)+B}} \quad (12)$$

176

177 α_a-depended A and B are shown in the quadratic equations of Figure 1. A and B versus α_a

178 are shown in Figure 2 and a quadratic fit is made based on the given ω and α_s at our site for A

179 and B individually shown as Eq. 13 and Eq. 14.

180 $$A = 0.123\times\alpha_a^2 - 0.128\times\alpha_a - 0.195 \quad (13)$$

181 $$B = -1.512\times\alpha_a^2 + 1.774\times\alpha_a + 2.637 \quad (14)$$

182

183 Based on Eq. 12, 13 and 14, $C(\lambda)$ at our site could be estimated for a given α_a and C_{ref}.

184 Schmid et al. (2006) indicated that C_{ref} at 532 nm is about 2.1 and 4.0 for pure or external mixtures

185 of soot and internal mixtures of soot, respectively. For the urban aerosols, the mean value 3.6 (Schmid

186 et al., 2006) was suggested and used in this study. Thus C was 2.95, 3.37, 3.56, 3.79, 3.99, 4.51 and

187 4.64 at 370, 470, 520, 590, 660, 880, and 950 nm, respectively.

188 As indicated in Coen et al. (2010), Virkkula correction and Arnott correction are not recommended

189 to be used to correct the absorption coefficient because the Virkkula correction does not consider all the

190 known artifacts and Arnott correction has technical limits due to the generation of new negative

191 absorption coefficient values. Although the determination of the *f* constant used in the WC2003 is not

192 clearly defined, it still shows a very good agreement with the Multi-Angle Absorption Photometer.

193 Similar to Arnott correction, SC2006 also introduces artifacts in the absorption wavelength dependence,

194 but to a lesser extent. And it also shows a very good agreement with the Multi-Angle Absorption

195 Photometer (Coen et al., 2010). Therefore, to estimate absorption coefficient of the aerosol in urban

196 Nanjing, both direct and indirect ways introduced above were employed in this study although the
197 indirect way could only address σ_{abs} at 532 nm. To make the comparison, 532 nm-σ_{abs} from
198 WC2003 and SC2006 was derived using the 520 and 590 nm-σ_{abs} according the following equations
199 (Angstrom. 1929):

200 $$\alpha_{abs,590/520nm} = -\frac{\log(\sigma_{abs,590nm} / \sigma_{abs,520nm})}{\log(590_{nm} / 520_{nm})} \quad (15)$$

201 $$\sigma_{abs,532nm} = \sigma_{abs,520nm} \times (\frac{532_{nm}}{520_{nm}})^{-\alpha_{abs,590/520nm}} \quad (16)$$

202

203 **3 Results and discussions**

204 **3.1 Temporal variations of the aerosol absorption coefficient**

205 We corrected the aerosol absorption coefficient (AAC) using three methods: an indirect correction
206 (IDC), Weingartner et al. (2003) (WC2003) and Schmid et al. (2006) (SC2006), in urban Nanjing
207 during the period from 2012 to 2013. It is worth noting that the indirect correction could only estimate
208 a single wavelength AAC (at 532 nm). To make it comparable, 532 nm-AACs from WC2003 and
209 SC2006 were calculated by Eq. 15 and Eq. 16. Temporal variations of AACs for the rest of
210 wavelengths from WC2003 and SC2006 corrections are similar to those of 532 nm-AAC (not shown).

211 Figure 3 presents the monthly variations of 532 nm-AAC in urban Nanjing in 2012 (Figure 3a)
212 and 2013 (Figure 3b) corrected by IDC, WC2003 and SC2006. The seasonal variations and the
213 magnitude of AAC at 532 nm agree closely between the direct and indirect corrections. The relatively
214 large difference in AACs between the direct and indirect corrections was in spring and summer (wet
215 seasons) both in 2012 and 2013. The difference is mostly caused by the shadowing effect *R* because
216 [BC] directly from AE-31 in Eq. 1 has not been corrected. The bias of the actual BC concentration from

217 [BC] is from the *R* as suggested by Eq.7 in Schmid et al. (2006) and Eq. 7 in Weingartner et al. (2003).
218 Thus, the results imply the importance of the shadowing effect in estimating AACs. The 2-year mean of
219 AAC at 532 nm averaged from the three corrections is about 43.23±28.13 Mm^{-1}, with a maximum and
220 a minimum of 273 Mm^{-1} and 1.28 Mm^{-1}, respectively, in urban Nanjing. AAC at 532 nm corrected by
221 IDC is the largest (44.38 Mm^{-1}), followed by that from WC2003 (43.38 Mm^{-1}) and SC2006 (41.93
222 Mm^{-1}). AACs in 2012 were a little smaller than those in 2013. The AAC in urban Nanjing has an
223 evident seasonal variation in both 2012 and 2013, generally higher in cold seasons and mostly lower in
224 warm seasons. Both precipitations and BC emissions may influence the seasonal variations in the AAC
225 to some extent. In summer, high frequent precipitation and low BC emissions (Zhang et al., 2009)
226 result in low BC concentrations, which is opposite to those in winter as suggested by Zhuang et al.
227 (2014b). Additionally, serious pollution episodes would lead to high levels of BC loadings, thus
228 considerably enhancing AACs. Although AACs are generally expected to be small in summer due to
229 low BC concentrations, AAC in June 2012 was substantially large (Fig. 3a). The monthly mean AAC
230 from SC2006 in this month is 51.89 M m^{-1}, which is about 1.5, 1.4 and 1.8 times to that in June in 2012,
231 in summer of 2012 and 2013, respectively. Such high AAC value is mainly resulted from a seriously
232 polluted event of BC during the period from 1st to 15th of June 2012. High BC loadings during this
233 period were due to a high intensity of biomass burning in northwestern region of Nanjing (Zhuang et al.
234 2014b). Fig. 3 shows that the monthly variation of AAC in 2012 was different from that in 2013. The
235 highest values of AAC were in June and October 2012 while in 2013, AAC was at the maximum in
236 winter (January, November and December). The large differences between the two years may be due to
237 the difference in pollution episodes, which eventually results in different seasonal variations of AACs
238 in Fig. 3.

AAC also has substantial diurnal variations (Figure 4). Its levels are high at rush hours (around 7-9 o'clock am and pm) but low in afternoon (around 1-3 o'clock pm) almost in all seasons in urban Nanjing in 2012 and 2013. At 7 o'clock am, averaged 532 nm-AAC was as large as about 50 Mm^{-1}, while at 2 o'clock pm, it was about 33 Mm^{-1}. Normally, large AACs during these periods of the day might be caused by the vehicle emissions (because the site is surround by several main roads with apparent traffic pollution as mentioned in Section 2) while the small AACs in afternoon was induced by well developed boundary layer (Zhuang et al. 2014b). Because the diurnal variations of AAC at 532 nm from IDC, WC2003 and SC2006 are similar (Fig 4a), one of them (SC2006) was selected to characterize the AAC's diurnal variation in detail (Fig. 4b). AAC's diurnal variation shows much stronger seasonality in 2013 than that in 2012 (Fig. 4b), which might be caused by substantial pollution episodes discussed above. In 2012, highly intensified biomass burning in early June near Nanjing resulted in a higher BC level (Zhuang et al., 2014b) and thus a larger AAC than those in 2013. Extremely high levels of AAC in winter in 2013 might also result from the poor air quality during these periods. In addition to its seasonality, the diurnal cycle itself could deviate from its normal pattern (peak at rush hours and trough in afternoon). Fig. 4b also shows that the standard deviations of AAC in 2012 (25.12 Mm^{-1}) are smaller than those in 2013 (28.58 Mm^{-1}) although their averaged values in 2012 and 2013 are closed to each other.

3.2 Frequencies of the aerosol absorption coefficient

Similar to the seasonal variations, the frequency patterns of AACs for the rest of wavelengths are consistent to those of 532 nm-AAC so the discussion is focused on the frequency of 532 nm-AAC only

261 to avoid duplication. Figure 5a shows the frequency distributions of 532 nm-AAC corrected by IDC,
262 WC2003 and SC2006 during the entire study period, which followed typical lognormal patterns. The
263 range from 15 to 65 Mm^{-1} dominated, accounting for more than 72% of the total data samples during
264 the entire period. The maximum frequencies of 10.07% (IDC), 10.57% (WC2003), and 10.89%
265 (SC2006) occurred at the ranges from 25 to 30 Mm^{-1}. The absolute differences between the directly and
266 indirectly corrected AACs are relatively larger at the range from 20 to 25 Mm^{-1} than those in other
267 ranges, possibly due to the influence of the shadowing effect in warming seasons as analyzed in
268 Section 3.1. Because of the consistency of the frequency patterns and order of magnitudes among the
269 three AACs, only the frequency of SC2006 AAC at 532 nm is presented in detail, illustrating the
270 inter-annual and seasonal variations of the frequency (Fig. 5b and Fig. 5c). Similar to the diurnal cycles,
271 frequency distributions of AAC in 2012 are more consistent with each other and more concentrated
272 than those in 2013. Frequencies at the ranges below 25 Mm^{-1} (28.57%) and above 70 Mm^{-1} (10.62%)
273 are smaller in 2012 compared to 2013 (31.09% and 15.47%, respectively). The peak frequency mostly
274 occurs at the smaller AAC range in summer while at the larger ones in other seasons. Additionally,
275 pollution episodes might alter the shape of the frequencies especially on seasonal or monthly scales.
276 High levels of aerosol loadings and its AACs would be observed during the period of the episodes,
277 which might lead to relatively higher frequency occurred at the larger AAC ranges. As shown in Fig. 5c,
278 frequencies of the values exceeding 65 Mm^{-1} were larger in fall compared to those in other seasons in
279 2012. Frequencies of the values larger than 55 Mm^{-1} were higher in winter compared to those in other
280 seasons in 2013. In summer 2012, frequencies of AAC ranging from 120 to 140 Mm^{-1} was larger
281 (0.94%) than those in spring (0.65%) and winter (0.58%) due to the biomass burning in northwestern
282 regions of Nanjing (Zhuang et al., 2014b). Over all, frequencies of AAC in 2013 show much more

283 seasonality compared to 2012. Large differences of the frequency distribution between 2012 and 2013
284 are mainly found in summer and winter.
285
286 **3.3 Periodic variation of the aerosol absorption coefficient**
287 In addition to diurnal cycles, AAC in Nanjing might have other periodicities during the study
288 period. Thus, Morlet wavelet is employed based on daily mean values of AAC at 532 nm corrected by
289 SC2006. Figure 6 shows the wavelet power spectrum (Figure 6a) and wavelet real part spectrum
290 (Figure 6b) of 532 nm-AAC. Cycles of 4-8 days and 9-17 days which are mostly statistically
291 significant at the confidence level of 95% dominate the local power spectrum, implying that variations
292 of AAC in urban Nanjing could also be affected by synoptic scale (weekly) weather systems and
293 quasi-two-week scale systems to some extent. The oscillations of AAC on the synoptic scale are found
294 in the period from late fall to early winter due to the quick and vigorous weather change. And
295 quasi-two-week scale oscillations of AAC are mainly in winter. Similar to AAC, visibility in Nanjing
296 also has synoptic scale and quasi-two-week scale periodic variations as indicated in Deng et al. (2011),
297 who suggested that the quasi-two-week oscillation might be a regional rather than local phenomenon in
298 China even in East Asia.
299
300 **3.4 Varied with wavelength of the aerosol absorption coefficient**
301 In the previous sections, single wavelength AAC (at 532 nm) is discussed as the AAC
302 distributions and seasonal variations are similar among different wavelengths. In this section,
303 wavelength depended AACs as well as absorption angstrom exponents (AAE) at 660/470 nm corrected
304 by WC2003 and SC2006 are further examined (Fig. 7). AACs from both WC2003 and SC2006

305 decrease with increasing wavelength (Fig. 7a). Although AAC at 532 nm from WC2003 is closed to
306 that from SC2006, substantial differences exist at other wavelengths. WC2003-AACs are smaller than
307 SC2006-AACs at shorter wavelengths (370 and 470 nm) but are larger than SC2006-ACCs in longer
308 wavelengths (from 590 nm to 950 nm). The averaged AACs range from 23.40 (at 950 nm) to 68.89
309 Mm^{-1} (at 370 nm) based on WC2003 and range from 17.56 (at 950 nm) to 82.07 Mm^{-1} (at 370 nm)
310 based on SC2006. Different correction methods on scattering effect C between WC2003 and SC2006
311 result in different variations of AAC with wavelengths because C in WC2003 is independent of
312 wavelength, and subsequently might lead to considerably different AAEs between these corrections
313 (Fig. 7b and 7c). Both Fig. 7b and 7c show that AAE at 660/470 nm from SC2006 is much larger than
314 that from WC2003, although they have similar seasonal variations. Annual mean 660/470 nm AAEs in
315 2012 and 2013 are 1.58 and 1.54 from SC2006 and 1.09 and 1.07 from WC2003. AAE from SC2006 is
316 about 1.5 times to that from WC2003. Additionally, AAE has strong seasonality with the high level in
317 winter and low level in summer, implying that absorbing aerosols in summer have larger sizes possibly
318 caused by large relative humidity (RH). Seasonal variations of AAE from AE-31 are similar to those
319 from CE-318 as compared with those in Zhuang et al. (2014a), who reported annual mean AAE of the
320 column aerosols from CE-318 being 1.44 at the site. Thus, this suggests that the scattering correction
321 method by Schmid et al. (2006) were more reasonable than that by Weingartner et al. (2003).
322
323 Table 1 summaries the optical properties of absorbing aerosols from AE-31 based on IDC,
324 WC2003 and SC2006. Two-years averaged values of AAC at 532 nm corrected by these three methods
325 are 44.38, 43.38 and 41.93 Mm^{-1}, respectively, in urban Nanjing. 660/470 nm AAE corrected by
326 WC2003 and SC2006 are 1.08 ± 0.20 and 1.56 ± 0.23, respectively. Annual mean AAC averaged from

all wavelengths is 40.78 Mm^{-1} (SC2006) and 41.41 Mm^{-1} (WC2003), while it is 41.47 Mm^{-1} (SC2006) ~ 42.97 Mm^{-1} (WC2006), averaged from visible wavelengths. The inter-annual difference suggests that AAC in 2012 is smaller than that in 2013, while AAE in 2012 is larger than that in 2013. The scattering correction of Weingartner et al. (2003) is different from that of Schmid et al. (2006), which would result in large variances of AAC at shorter (<520 nm) or longer (>590 nm) wavelengths, causing large difference of AAE between the two methods. However, AACs at 532 nm or averaged from all wavelengths from WC2003 and SC2006 are closed to each other. Many studies on aerosol optical properties have been carried out by model simulations and observations. Most of them focused on the optical depth and single scattering albedo of column (from surface to the top of the atmosphere) aerosols (Zhuang et al., 2014a), few on the aerosol absorption coefficient, even less on AAC in urban areas of YRD. Annual AAE at 660/470 nm corrected by SC2006 agree well with the one observed by CE-318 at the site. Xu et al. (2004) pointed out that AAC at 565 nm was 6 ± 11 Mm^{-1} in Gobi desert (Yulin) in China in 1999. In Beijing, capital of China, annual AAC at 532 nm was about 17.54 ± 13.44 Mm^{-1} at a rural site (Shangdianzi: SDZ) in 2003 and 2004 (Yan et al., 2008) while it was about 45 ± 39 Mm^{-1} at an urban site from 2005 to 2006 (He et al., 2009). AAC at 532 nm at rural site of YRD (Lin'an) was about 44.3 ± 19.7 Mm^{-1} in 2004 (Yan, 2006). In the semi-arid area in Northeast China (Tongyu), AAC at 520 nm was only about 7.28 ± 5.87 Mm^{-1} from 2010 to 2011 (Wu et al., 2012). In Pearl River Delta (PRD) of China, annual AAC at 532 nm was as large as 82 ± 23 Mm^{-1} at urban areas from 2004 to 2007 (Wu et al., 2009). Levels of annual AAC in urban Nanjing, to some extent, were comparable to those in other Chinese urban or rural sites. Comparisons suggest that AAC in urban Nanjing (YRD) were much lower than those in PRD but higher than those in non-urban sites of North China (Shangdianzi, Tongyu and Yulin). In YRD, annual AAC in urban Nanjing was as large as that in rural

areas (Lin'an), which is similar to the BC concentrations there (Zhuang et al., 2014b).

3.5 Aerosol absorption coefficient in different wind directions

In addition to local emissions, the meteorological factors such as the prevailing wind could also affect the AAC and AAE in urban Nanjing. Backward trajectories analysis shown in Fig. 8a and 8b indicated that Nanjing could be affected by local air flow and long-distance air flows mostly from northwestern, northern, eastern, southeastern and southern direction both in 2012 and 2013, implying that the prevailing winds might have weaker inter-annual variations compared to the aerosols. Air flows from northern directions account for about the half of the totals while the local air flow and the flows from the oceans account for about 13%, ~19% and 15%, respectively. Frequencies of air flows from south and northwest China are relatively smaller. Rose plot of near surface wind around the site (32^{o} N, 118.76^{o} E, 8 m tall) during the entire study period (Fig. 8c) suggests that the distributions of the near surface wind directions somewhat agree with those from the backward trajectory analysis. However, the winds near the surface come from the southeastern to eastern directions more frequently, accounting for more than 35% of the totals. Probabilities of the wind from south to west account for the least (Fig. 8c). The wind speed is mostly concentrated in the values from 2 to 6 m/s in Nanjing during the period.

As mentioned above, wind direction shifting over different seasons might be another important factor in determining the aerosol AAC and AAE. Zhuang et al. (2014b) indicated that high BC loadings in fall and summer of 2012 were observed at the site when winds were from northeastern and northwestern directions, in which air masses might be highly polluted, thus leading to considerably

large AAC. Figure 9 presents the levels of AAC at 532 nm and AAE at 660/470 nm corrected by SC2006 associated with different clusters (shown in Figure 8) in urban Nanjing both in 2012 and 2013. Considerable air pollutants are derived from local and sub-regional emissions as presented in cluster 6 (Fig. 9a and 8a) in 2012 and in cluster 3 (Fig. 9b and 8b) in 2013, with averaged values of 56.13 Mm^{-1} and 65.38 Mm^{-1}, respectively. Air masses from the oceans and south China (sea) (cluster 7, 8 and 9 in Fig. 8a and 8b) were relatively clean, leading to smaller AACs in Nanjing (Fig. 9a and 9b), with averaged values of 33.28 Mm^{-1} in 2012 and 30.1 Mm^{-1} in 2013. The air masses from the remote sites (cluster 2, 3 and 4 in 2012 in Fig. 8a and cluster 1, 4 and 5 in 2013 in Fig. 8b) could also bring the clean air and then might result in relatively low levels of AACs in Nanjing. Previous analysis indicates that prevailing winds have weak inter-annual variations. Thus, substantial differences (about 15 Mm^{-1}) between AAC from cluster 3 (or cluster 5) in 2012 and cluster 2 (or cluster 6) in 2013 might mostly result from the regional pollution episodes in North China in 2013. In addition to AAC, AAE levels are also somewhat affected by different air flows. Fig. 9c and 9d suggest that AAE in urban Nanjing is relatively small when the air masses come from the oceans (cluster 7 and 9) possibly due to the affection of moisture while is larger when the flows are from the areas of higher latitudes. Local AAEs are 1.52 (in cluster 6 in Fig. 9c) in 2012 and 1.62 (in cluster 3 in Fig. 9d) in 2013, which are closed to the annual mean value of 1.56.

3.6 Relationship between aerosol absorption coefficient and its absorption angstrom exponent

Aerosol absorption coefficient is directly determined by the loadings of absorbing aerosols. Additionally, both aerosol size's distribution and relative humidity (RH), especially the former, are closely related to the variation in AAC. Figure 10 shows the relationships among AAC at 532 nm

393 corrected by SC2006, AAE at 660/470 nm corrected by SC2006 and RH. It suggests that changes in
394 aerosol mass (or specific) absorption coefficients (MAC for short, defined as ratios of AAC to BC
395 loading, in m^2/g) at 532 nm are closely relative to the variations of AAE. High levels of MAC mostly
396 appear in the ranges with large AAE, implying that absorbing aerosols with smaller sizes might absorb
397 more solar radiation because the fine particles have much larger specific surface areas compared to
398 coarse ones. The linear correlation coefficient between MAC and AAE exceeds 0.92 in urban Nanjing
399 during the study period (Fig. 10a). Changes in AAE somewhat are influenced by the variations of RH.
400 Fig. 10a also indicates that large AAEs are mostly found when the RH is low and vice versa. Generally,
401 moist air is in favor of hygroscopic growth of the aerosols, thus resulting in smaller AAE
402 (corresponding to large size of the aerosols). These results could further explain why AAE in urban
403 Nanjing is relatively small when the air masses come from the oceans as discussed in the previous
404 section (Fig. 8 and 9). In addition to AAE, AAC is also affected by RH, as shown in Fig. 10b for
405 AAC-RH relationship in different AAE levels. Large AAC appears in the range with large AAE while
406 coarser aerosols (AAE<1.3) could only be found in the condition with relatively large RH. Changes in
407 AAC with RH are different within different bins of AAE. Polynomial fitting between AAC and RH
408 indicates that the peaks of AAC mainly concentrate at the value 65% of RH for the finer (AAE>1.6)
409 absorbing aerosols (unimodal). While for coarser ones, quasi-bimodal distribution of AAC is found.
410 High levels of AAC within the ranges of AAE from 1.3 to 1.6 mostly appear at the value of 40% and
411 80%. Large AACs within the ranges of AAE below 1.3 are mostly found in the value of 65% and 85%.
412 Polynomial correlation coefficients of these three fittings are 0.25, 0.16 and 0.38, respectively, which is
413 statistically significant at the confident levels of 99%, 99% and 90%.
414

3.7 Aerosol absorption coefficient during pollution episodes

The previous analysis indicates that extremely high levels of aerosol could be observed due to serious pollution episodes, which might affect the temporal and frequency distributions of AAC in urban Nanjing. Diurnal variation of BC in the period from 1st to 15th June in 2012 was altered significantly from its normal distribution (Zhuang et al., 2014b), so does the AAC in this period as expected. The mean value of AAC at 532 nm from January 2012 to December 2013 shown in Table 1 is about 43 Mm^{-1}. However, the daily mean AACs far outstripping the value 90 Mm^{-1}, ~2 times of the annual mean, could be found frequently especially in Mar, June, November in 2012 and in January, November, December in 2013 (Figure 11). The largest values of the daily AAC at 532 corrected by SC2006 in these months all exceeded 100 Mm^{-1}, especially on 10th June 2012 and 4th December 2013 on which AACs were as large as 147.19 and 149.38 Mm^{-1}, respectively. The high levels of AAC in June 2012 mainly result from biomass burning in the northwestern region of Nanjing (belongs to local pollution in cluster 6 of Fig. 8a), as discussed in Zhuang et al. (2014b). Levels and distributions of Aerosol optical depth (AOD) from satellite (MODIS) retrievals (not shown) indicate that high aerosol loadings or absorption coefficients during the periods from 9th to 13th January 2013 and from 1st to 8th December 2013 might possibly be caused by large scale regional pollutions over East to North China (Nanjing is included). The reasons leading to high aerosol pollutions in Nanjing during the sampling period would be analyzed in detailed in further studies, so does the characteristics of AAC and AAE in pollution episodes.

4 Conclusions

In this study, the near-surface aerosol absorption coefficient (AAC) and angstrom exponent (AAE)

437 in urban Nanjing in 2012 and 2013 are investigated based on the measurements from the 7-channel
438 Aethalometer (model AE-31, Magee Scientific, USA). As suggested by Collaud Coen et al. (2010),
439 Weingartner et al. (2003) (WC2003 for short) and Schmid et al. (2006) (SC2006 for short) corrections
440 are used to assess the AAE at 660/470 nm and wavelength depended AAC. The indirect correction
441 (IDC) is also used to estimate the 532 nm-AAC based on the observed conversion factor in Nanjing.
442 Analysis in AAC is focused on at wavelength 532 nm to facilitate the comparisons between the directly
443 and indirectly correction of AACs, as the temporal variation and frequency distribution of ACC at each
444 wavelength are similar to those at 532 nm.

445 The direct and indirect corrections closely agree in terms of the temporal variation and magnitude
446 of AAC at 532 nm in the entire study period except in spring and summer possibly due to the
447 shadowing effect which is strong in these seasons. AAC at 532 nm corrected by IDC is the largest,
448 followed by that from WC2003 and SC2006. The mean AAC at 532 nm averaged from these three
449 corrections is about 43.23±28.13 Mm^{-1} in urban Nanjing, with substantial seasonal and diurnal
450 variations. Higher AACs often appeared in cold seasons (at rush hours) while lower ones in summer (in
451 afternoon). Small AAC in summer (in afternoon) were partially due to large scavenging efficiency and
452 smaller emission rates of the aerosols (the well developed boundary layers). AAC in urban Nanjing is
453 much lower than that in Pearl River Delta but higher than that in non-urban sites of North China.
454 Within YRD, annual AAC in urban Nanjing is as large as that in rural areas (Lin'an). Wavelet analysis
455 suggests that variations of AAC in urban Nanjing might have cycles of 4-8 days and 9-17 days due to
456 the affection of synoptic scale (weekly) weather systems and quasi-two-week scale systems. AACs
457 follow a typical lognormal pattern in terms of the frequency distribution. For AAC at 532 nm, the range
458 from 15 to 65 Mm^{-1} dominates, accounting for more than 72% of the total data samples in the entire

study period. And the maximum frequencies of about 10% ~11% occur at the ranges from 25 to 30 Mm^{-1}. Both diurnal variations and frequency distributions of AAC shows more evident seasonality in 2013 than those in 2012 possibly because of the influences of the pollution episodes.

AAC in urban Nanjing has been affected by serious pollution episodes locally and regionally, thus much enhanced AACs have been observed frequently. AACs are expected to be small in summer due to low BC concentrations at the time. However, AACs were substantially large (exceeding 50 Mm^{-1}) in June 2012 due to a high intensity of biomass burning around Nanjing during 1-15 June 2012. Extremely high AACs in winter in 2013 might be caused by large scale regional pollutions over East to North China. Hence, AAC diurnal cycle, frequency, and their seasonal variations were altered. High AACs appeared at mid-night during the period 1-15 June 2012, instead of in the morning as usual. Frequency of AAC followed a quasi-bimodal distribution in winter in 2013 and its values at the AAC range larger than 55 Mm^{-1} were higher compared to those in other seasons in 2013. The durations of sample spot in the filter (or the speeds of the tape advance) show significant differences among different AAC levels. It is much shorter (mostly no more than 5 hours) in the periods of pollution than those in clean days (more than 9 hours).

The AAC at the site generally decreases with increasing wavelength. Although AAC at 532 nm from WC2003 is closed to the one from SC2006, its decline rate is smaller than SC2006's because the scattering correction C from WC2003 is independent of wavelength. Thus, AAE at 660/470 nm from SC2006 (=1.56) is much larger than that from WC2003 (=1.08). The scattering correction by Schmid et al. (2006) appears more reasonable than that by Weingartner et al. (2003), compared to the column AAE at 675/440 nm by CE-318 at the site. AAE also has strong seasonality, high in winter and low in summer, possibly related to the variation in relative humidity (RH) (Zhuang et al., 2014a).

Wind direction shifting over different seasons might be another factor controlling the aerosol AAC and AAE. Backward trajectories indicate that Nanjing could be affected by local air flow (13% ~19%) and long-distance air flows mostly from northwestern, northern (>50%), eastern, southeastern and southern directions. Considerable air pollutions in urban Nanjing are due to local and sub-regional emissions. Air masses from the oceans and remote areas are relatively clean with low AACs. During the pollution episodes in North China in 2013, a large number of aerosols was transported to Nanjing, greatly enhancing AAC at the site. AAE at the site is usually low when the air masses come from the oceans while it is high when the air flows from the areas of higher latitudes.

AAC generally increases with increasing AAE under the condition of fixed aerosol loadings in urban Nanjing. The linear correlation coefficient between aerosol mass absorption coefficients (MAE) at 532 nm and AAC exceeds 0.92 during the entire study period. High levels of MAC mostly appear in the ranges with large AAE because the fine particles have much larger specific surface area compared to coarse ones. Changes in AAE and AAC are somewhat influenced by the variations of RH. Large AAEs are mostly found when the RH is low and vice versa. Changes in AAC with RH are different within different bins of AAE. Unimodal and quasi-bimodal distributions of AAC vary with RH for finer (AAE>1.6) and coarser (AAE<1.6) absorbing aerosols, respectively. The peak AAC mainly concentrates at RH= 65% for the aerosols with AAE<1.6. For the aerosols with 1.3<AAE<1.6, the maximum AACs appear around RH being 40% and 80%, while for AAE<1.3, AAC peaks around RH being 65% and 85%.

Acknowledgements: This work was supported by the National Key Basic Research Development Program of China (2014CB441203 and 2011CB403406), the Young Scientists Fund of the National

Natural Science Foundation of China (41205111), the New Teachers' Fund for Doctor Stations, Ministry of Education (20120091120031), the Fundamental Research Funds for the Central Universities (20620140744), FP7 project: REQUA (PIRSES-GA-2013-612671), and a project Funded by the Priority Academic Program Development of the Jiangsu Higher Education Institutions (PAPD). The authors would like to thank all members in the AERC of Nanjing University for maintaining instruments. HYSPLIT model was supplied by NOAA: http://ready.arl.noaa.gov/HYSPLIT_traj.php.

5 References

Angström, A.: On the atmospheric transmission of sun radiation and on dust in the air, Geogr. Ann., 11, 156–166, 1929.

Arnott, W. P., Hamasha, K., Moosmuller, H., Sheridan, P. J., and Ogren, J. A.: Towards aerosol light-absorption measurements with a 7-wavelength aethalometer: evaluation with a photoacoustic instrument and 3-wavelength nephelometer, Aerosol Sci. Tech., 39, 17–29, doi:10.1080/027868290901972, 2005.

Bai, H. T., Chen, Y. H., Wang, H. Q., Zhang, Q., Guo, N., Wang, S., Pan, H., and Zhang, P.: Seasonal variation of aerosol optical properties at AERONET of the semi-arid region in Loess Plateau, Arid Land Geogr., 34, 1–8, 2011.

Bellouin, N., Boucher, O., Tanré, D., and Dubovik, O.: Aerosol absorption over the clear-sky oceans deduced from POLDER-1 and AERONET observations, Geophys. Res. Lett., 30, 1748, doi:10.1029/2003GL017121, 2003.

Cai, H. K., Zhou, R. J., Fu, Y. F., Zheng, Y. Y., and Wang, Y. J.: Cloud-aerosol lidar with or thogonal polarization detection of aerosol optical properties after a crop burning case, Clim. Environ. Res.,

16, 469–478, 2011.

Collaud Coen, M., Weingartner, E., Apituley, A., Ceburnis, D., Fierz-Schmidhauser, R., Flentje, H., Henzing, J. S., Jennings, S. G., Moerman, M., Petzold, A., Schmid, O., and Baltensperger, U.: Minimizing light absorption measurement artifacts of the Aethalometer: evaluation of five correction algorithms, Atmos. Meas. Tech., 3, 457–474, doi:10.5194/amt-3-457-2010, 2010.

Deng, J. J., Wang, T. J., Jiang, Z. Q., Xie, M., Zhang, R. J., Huang, X. X., and Zhu, J. L.: Characterization of visibility and its affecting factors over Nanjing, China, Atmos. Res., 101, 681–691, doi:10.1016/j.atmosres.2011.04.016, 2011.

Forster, P., Ramaswamy, V., Artaxo, P., Berntsen, T., Betts, R., Fahey, D. W., Haywood, J., Lean, J., Lowe, D. C., Myhre, G., Nganga, J., Prinn, R., Raga, G., Schulz, M., and Van Dorland, R.: Changes in atmospheric constituents and in radiative forcing, in: Climate Change 2007: The Physical Science Basis. Contribution of Working Group I to the Fourth Assessment Report of the Intergovernmental Panel on Climate Change, edited by: Solomon, S. et al., Cambridge Univ. Press, Cambridge, UK, 129–234, 2007.

Hansen, A. D. A., Rosen, H., and Novakov, T.: The aethalometer: an instrument for the real time measurements of optical absorption by aerosol particles, Sci. Total Environ., 36, 191–196, 1984.

He, X., Li, C. C., Lau, A. K. H., Deng, Z. Z., Mao, J. T., Wang, M. H., and Liu, X. Y.: An intensive study of aerosol optical properties in Beijing urban area, Atmos. Chem. Phys., 9, 8903–8915, doi:10.5194/acp-9-8903-2009, 2009.

Holler, R., Ito, K., Tohno, S., and Kasahara, M.: Wavelength-dependent aerosol single scattering albedo: measurements and model calculations for a coastal site near the sea of Japan during ACE-Asia, J. Geophys. Res., 108, 8648, doi:10.1029/2002JD003250, 2003.

547 Jacobson, M. Z.: Control of fossil-fuel particulate black carbon and organic matter, possibly the most
548 effective method of slowing global warming, J. Geophys. Res., 107, 4410,
549 doi:10.1029/2001JD001376, 2002.
550 Kiehl, J. T. and Briegleb, B. P.: The relative roles of sulfate aerosols and greenhouse gases in climate
551 forcing, Science, 260, 311–314, 1993.
552 Li, Z. Q., Lee, K. H., Wang, Y. S., Xin, J. Y., and Hao, W. M.: First observation-based estimates of
553 cloud-free aerosol radiative forcing across China, J. Geophys. Res., 115, D00K18,
554 doi:10.1029/2009JD013306, 2010.
555 Liao, H. and Seinfeld, J. H.: Global impacts of gas-phase chemistry-aerosol interactions on direct
556 radiative forcing by anthropogenic aerosols and ozone, J. Geophys. Res., 110, D18208,
557 doi:10.1029/2005JD005907, 2005.
558 Menon, S., Hansen, J., Nazarenko, L., and Luo, Y. F.: Climate effects of black carbon aerosols in China
559 and India, Science, 297, 2250–2253, doi:10.1126/science.1075159, 2002.
560 Penner, J. E., Andreae, M., Annegarn, H., Barrie, L., Feichter, J., Hegg, D., Jayaraman, A., Leaitch, R.,
561 Murphy, D., Nganga, J., and Pitari, G.: Aerosols, their direct and indirect effects, in: Climate
562 Change 2001: The Scientific Basis. Contribution of Working Group I to the Third Assessment
563 Report of the Intergovernmental Panel on Climate Change, edited by: Houghton, J. T. et al.,
564 Cambridge University Press, Cambridge, UK and New York, NY, USA, 289–348, 2001.
565 Petzold, A., Kopp, C., and Niessner, R.: The dependence of the specific attenuation cross-section on
566 black carbon mass fraction and particle size, Atmos. Environ., 31, 661–672, 1997.
567 Schmid, O., Artaxo, P., Arnott, W. P., Chand, D., Gatti, L. V., Frank, G. P., Hoffer, A., Schnaiter, M., and
568 Andreae, M. O.: Spectral light absorption by ambient aerosols influenced by biomass burning in the

569 Amazon Basin. I: Comparison and field calibration of absorption measurement techniques, Atmos.
570 Chem. Phys., 6, 3443–3462, doi:10.5194/acp-6-3443-2006, 2006.
571 Streets, D. G., Gupta, S., Waldhoff, S. T., Wang, M. Q., Bond, T. C., and Bo, Y. Y.: Black carbon
572 emissions in China, Atmos. Environ., 35, 4281–4296, doi:10.1016/S1352-2310(01)00179-0, 2001.
573 Virkkula, A., Makela, T., Hillamo, R., Yli-Tuomi, T., Hirsikko, A., Hameri, K., and Koponen, I. K.: A
574 simple procedure for correcting loading effects of aethalometer data, J. Air Waste Manage., 57,
575 1214–1222, doi:10.3155/1047-3289.57.10.1214, 2007.
576 Wang, Y., Che, H. Z., Ma, J. Z., Wang, Q., Shi, G. Y., Chen, H. B., Goloub, P., and Hao, X. J.: Aerosol
577 radiative forcing under clear, hazy, foggy, and dusty weather conditions over Beijing, China,
578 Geophys. Res. Lett., 36, L06804, doi:10.1029/2009GL037181, 2009.
579 Weingartner, E., Saathoff, H., Schnaiter, M., Streit, N., Bitnar, B., and Baltensperger, U.: Absorption of
580 light by soot particles: determination of the absorption coefficient by means of aethalometers, J.
581 Aerosol Sci., 34, 1445–1463, doi:10.1016/S0021-8502(03)00359-8, 2003.
582 Wu, D., Mao, J. T., Deng, X. J., Tie, X. X., Zhang, Y. H., Zeng, L. M., Li, F., Tan, H. B., Bi, X. Y.,
583 Huang, X. Y., Chen, J., and Deng, T.: Black carbon aerosols and their radiative properties in the
584 Pearl River Delta region, Sci. China Ser. D, 52, 1152–1163, doi:10.1007/s11430-009-0115-y, 2009.
585 Wu, D.,Wu, C., Liao, B., Chen, H.,Wu, M., Li, F., Tan, H., Deng, T., Li, H., Jiang, D., and Yu, J. Z.:
586 Black carbon over the South China Sea and in various continental locations in South China, Atmos.
587 Chem. Phys., 13, 12257–12270, doi:10.5194/acp-13-12257-2013, 2013.
588 Wu, Y. F., Zhang, R. J., Pu, Y. F., Zhang, L. M., Ho, K. F., and Fu, C. B.: Aerosol optical properties
589 observed at a semi-arid rural site in northeastern China, Aerosol Air Qual. Res., 12, 503–514, 2012.
590 Xia, X. A., Li, Z. Q., Holben, B., Wang, P., Eck, T., Chen, H. B., Cribb, M., and Zhao, Y. X.: Aerosol

591 optical properties and radiative effects in the Yangtze Delta region of China, J. Geophys. Res., 112,
592 D22S12, doi:10.1029/2007JD008859, 2007.
593 Xiao, Z. Y., Jiang, H., Chen, J., Wang, B., and Jiang, Z. S.: Monitoring the aerosol optical properties
594 over Hangzhou using remote sensing data, Acta Sci. Circumst., 31, 1758–1767, 2011.
595 Xu, J., Bergin, M. H., Greenwald, R., Schauer, J. J., Shafer, M. M., Jaffrezo, J. L., and Aymoz, G.:
596 Aerosol chemical, physical, and radiative characteristics near a desert source region of Northwest
597 China during ACE-Asia, J. Geophys. Res., 109, D19S03, doi:10.1029/2003JD004239, 2004.
598 Yan, P.: Study on the aerosol optical properties in the background regions in the East part of China,
599 PhD Thesis, Peking University, China, 2006.
600 Yan, P., Tang, J., Huang, J., Mao, J. T., Zhou, X.J., Liu, Q., Wang, Z. F., and Zhou, H. G.: The
601 measurement of aerosol optical properties at a rural site in Northern China, Atmos. Chem. Phys., 8,
602 2229–2242, doi:10.5194/acp-8-2229-2008, 2008.
603 Zhang, Q., Streets, D. G., Carmichael, G. R., He, K. B., Huo, H., Kannari, A., Klimont, Z., Park, I. S.,
604 Reddy, S., Fu, J. S., Chen, D., Duan, L., Lei, Y., Wang, L. T., and Yao, Z. L.: Asian emissions in
605 2006 for the NASA INTEX-B mission, Atmos. Chem. Phys., 9, 5131–5153,
606 doi:10.5194/acp-9-5131-2009, 2009.
607 Zhou, B., Zhang, L., Cao, X. J., Han, X., Zhang, W., and Feng, G. H.: Analyses on atmospheric aerosol
608 optical properties with lidar data in Lanzhou suburb, Plateau Meteorol., 30, 1011–1017, 2011.
609 Zhu, J., Wang, T., Talbot, R., Mao, H., Hall, C. B., Yang, X., Fu, C., Zhuang, B., Li, S., Han, Y., and
610 Huang, X.: Characteristics of atmospheric Total Gaseous Mercury (TGM) observed in urban
611 Nanjing, China, Atmos. Chem. Phys., 12, 12103–12118, doi:10.5194/acp-12-12103-2012, 2012.
612 Zhuang, B. L., Li, S., Wang, T. J., Deng, J. J., Xie, M., Yin, C. Q., and Zhu, J. L.: Direct radiative

forcing and climate effects of anthropogenic aerosols with different mixing states over China, Atmos. Environ., 79, 349–361, doi:10.1016/j.atmosenv.2013.07.004, 2013a.

Zhuang, B. L., Liu, Q., Wang, T. J., Yin, C. Q., Li, S., Xie, M., Jiang, F., and Mao, H. T.: Investigation on semi-direct and indirect climate effects of fossil fuel black carbon aerosol over China, Theor. Appl. Climatol., 114, 651–672, doi:10.1007/s00704-013-0862-8, 2013b.

Zhuang, B. L., Wang, T. J., Li, S., Liu, J., Talbot, R., Mao, H. T., Yang, X. Q., Fu, C. B., Yin, C. Q., Zhu, J. L., Che, H. Z., and Zhang, X. Y.: Optical properties and radiative forcing of urban aerosols in Nanjing, China, Atmos. Environ., 83, 43–52, 2014a.

Zhuang, B. L., Wang, T. J., Liu, J., Li, S., Xie, M., Yang, X. Q., Fu, C. B., Sun, J. N., Yin, C. Q., Liao, J. B., Zhu, J. L., and Zhang, Y.: Continuous measurement of black carbon aerosol in urban Nanjing of Yangtze River Delta, China, Atmos. Environ., 89, 415–424, 2014b.

Figure captions:

Figure 1. Double logarithmic plot of C versus λ for α_a=1 (orange), 1.5 (green), 2 (blue) and 2.5 (violet), respectively.

Figure 2. Variations of the coefficients A and B with α_a.

Figure 3. Monthly variations of the aerosol absorption coefficients (Mm^{-1}) at 532 nm in urban Nanjing in 2012 (a) and 2013 (b). The 10th, 25th, median, 75th, 90th percentile values of the coefficient corrected by SC2006 are presented as box plot. The monthly means of the coefficients corrected by indirect way (red), WC2003 (blue) and SC2006 (light green) are presented as line-markers.

Figure 4. Diurnal variations of the aerosol absorption coefficients at 532 nm in urban Nanjing. (a) the two-year (2012-2013) coefficients corrected by indirect way (red), WC2003 (blue) and SC2006 (light

635 green) and (b) the coefficients corrected by SC2006 in separate seasons of 2012 and 2013. Mar, April
636 and May represent the spring, June, July and August represent the summer, September, October and
637 November represent the fall, and January, February and December in 2012 (2013) represent the winter
638 in 2012 (2013).
639 Figure 5. Frequency distributions of the aerosol absorption coefficients at 532 nm in urban Nanjing. (a)
640 the two-year (2012-2013) coefficients corrected by indirect way (red), WC2003 (blue) and SC2006
641 (light green), (b) the coefficients corrected by SC2006 in separate year 2012 (solid bar) and 2013 (erase
642 bar), and (c) the coefficients corrected by SC2006 in separate seasons of separate year.
643 Figure 6. The local wavelet power spectrum (a) and wavelet real part spectrum (b) of the aerosol
644 absorption coefficient at 532 nm using the Morlet wavelet. The left axis is the wavelet scale (in day)
645 corresponding to the Fourier period on the right axis. The bottom axis is local time (month). The filled
646 parts in Fig. 6a indicate passing 95% confidence level test, and the parts below the dashed line are
647 unlikelihood.
648 Figure 7. Dependence of the aerosol absorption coefficient corrected by WC2003 (blue) and SC2006
649 (green) on the wavelength in urban Nanjing during the period from 2012 to 2013 (Fig. a). Annual (dash
650 lines) and seasonal (bars with error bar) absorption angstrom exponents at 660/470 nm from WC2003
651 (light blue) and SC2006 (green) both in 2012 (Fig. b) and 2013 (Fig. c).
652 Figure 8. Clusters of 96-h back trajectories arriving at the study site at 100 m in 2012 (a) and 2013 (b)
653 simulated by HYSPIT model and the probability distributions of 6 hours interval near surface wind
654 speed in different wind directions in Nanjing (c).
655 Figure 9. The 10%, 25%, 50%, 75% and 90% percentile values of the aerosol absorption coefficient (a,
656 b) and absorption angstrom exponent (c, d) in each cluster of back trajectories in 2012 (Fig. 8a) and

2013 (Fig. 8b).

Figure 10. Relationships between the aerosol mass (or specific) absorption coefficient (m^2/g) and its angstrom exponent (a, scatter plots) and the effects of relative humidity on the aerosol absorption coefficient (a, in color and b) in different absorption angstrom exponent levels.

Figure 11. Time series of daily mean aerosol absorption coefficient at 532 nm corrected by IDC (red), WC2003 (blue) and SC2006 (green) in the period from 2012 to 2013.

Tables:

Table 1. Statistical values of annual aerosol absorption coefficient (Mm^{-1}) and absorption angstrom exponent in urban Nanjing

Year	Schemes	All wave AAC		Visible wave AAC		532 nm- AAC		AAE (660/470 nm)	
		Average	Std	Average	Std	Average	Std	Average	Std
2012	IDC	/	/	/	/	42.99	26.55	/	/
	SC2006	39.70	35.26	40.34	27.10	41.02	25.70	1.58	0.20
	WC2003	40.48	31.26	41.97	27.29	42.44	26.59	1.09	0.20
2013	IDC	/	/	/	/	45.81	30.22	/	/
	SC2006	41.91	38.64	42.66	30.61	42.87	29.14	1.54	0.25
	WC2003	42.39	34.41	43.99	30.79	44.34	30.15	1.07	0.21
2-year	IDC	/	/	/	/	44.38	28.45	/	/
period	SC2006	40.78	36.97	41.47	28.89	41.93	27.47	1.56	0.23
	WC2003	41.41	32.86	42.97	29.08	43.38	28.41	1.08	0.20

IDC: The coefficients from the indirect correction.

SC2006: The coefficients corrected by Schmid et al. (2006).

WC2003: The coefficients corrected by Weingartner et al. (2003).

AAC: Aerosol absorption coefficients.

AAE: Absorption angstrom exponent.

Figures:

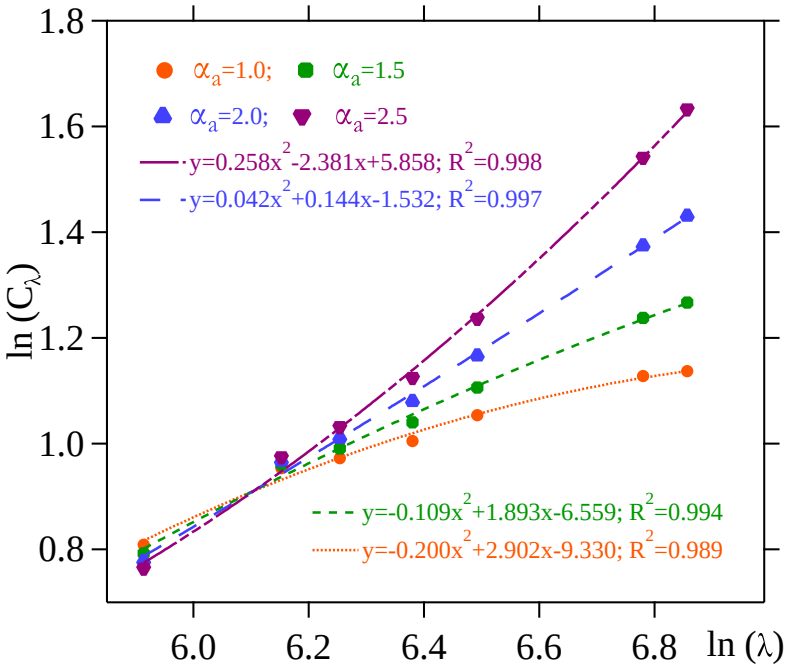

Figure 1.

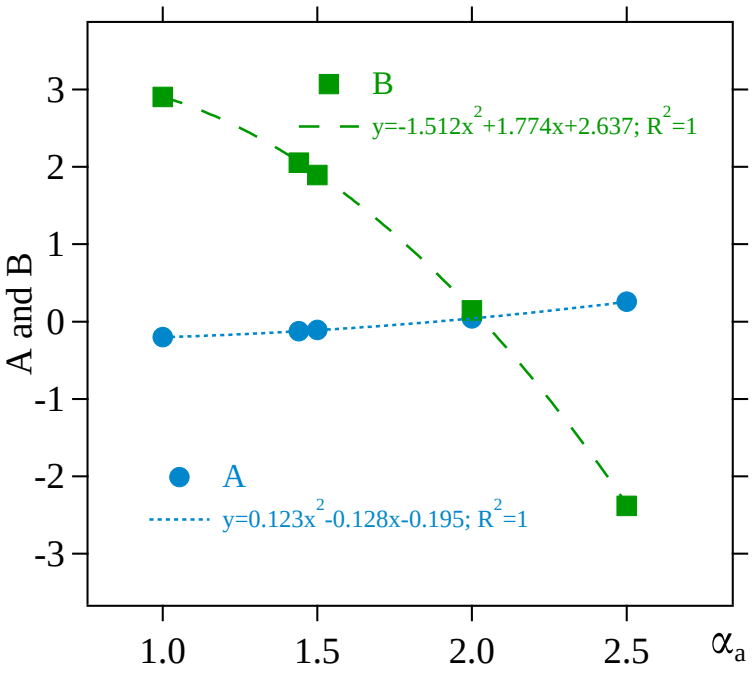

Figure 2.

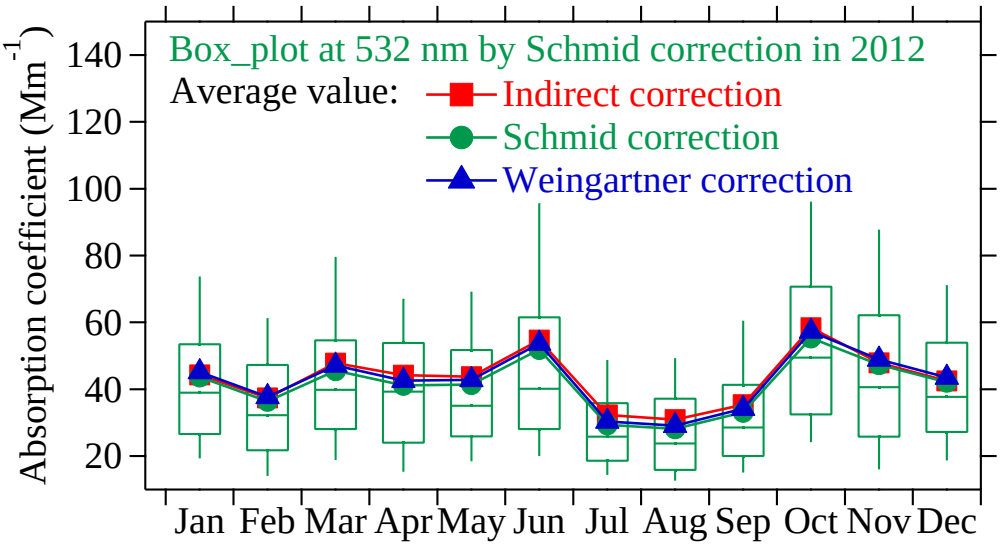
Box_plot at 532 nm by Schmid correction in 2012
Average value:
Indirect correction
Schmid correction
Weingartner correction
Absorption coefficient (Mm-1)
140
120
100
80
60
40
20
Jan Feb Mar Apr May Jun Jul Aug Sep Oct Nov Dec

a)

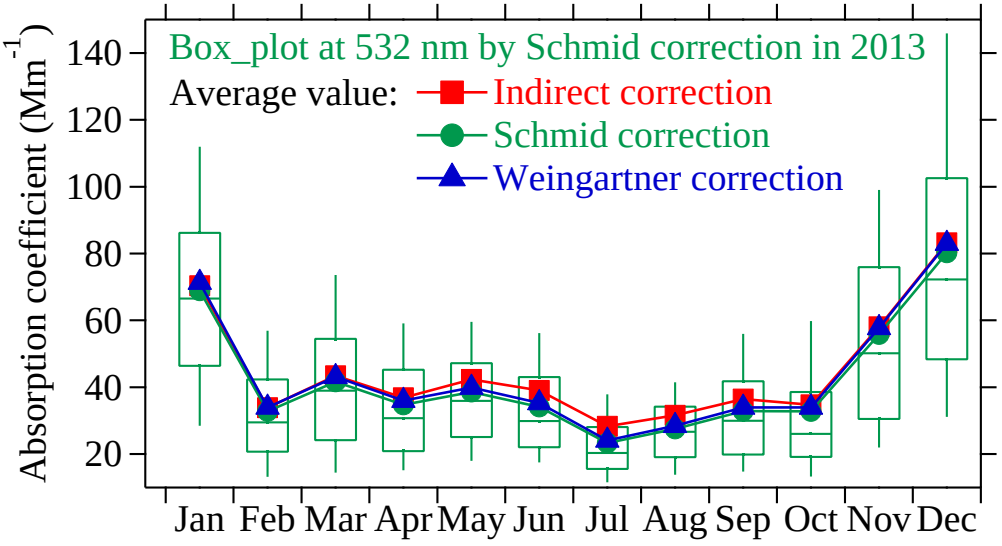
Box_plot at 532 nm by Schmid correction in 2013
Average value:
Indirect correction
Schmid correction
Weingartner correction
Absorption coefficient (Mm-1)
140
120
100
80
60
40
20
Jan Feb Mar Apr May Jun Jul Aug Sep Oct Nov Dec

b)

Figure 3

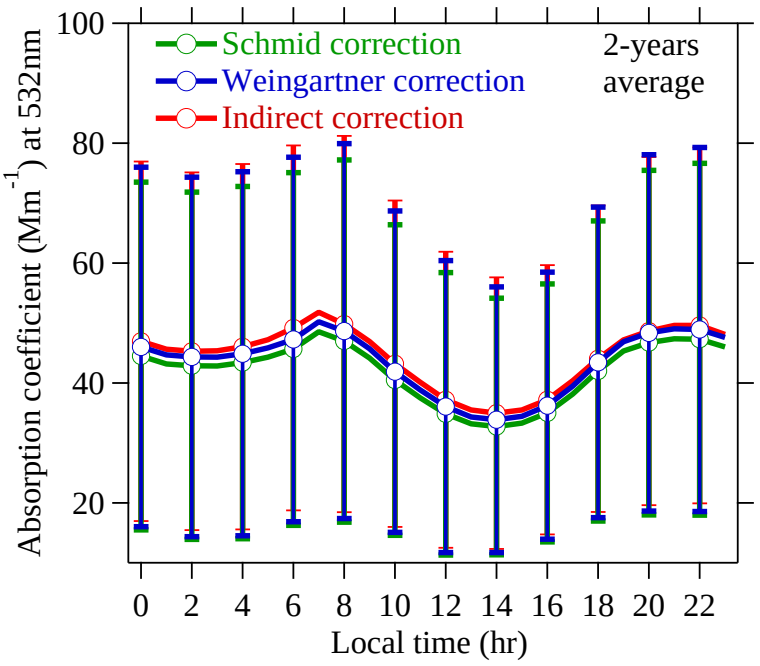
Schmid correction
Weingartner correction
Indirect correction
2-years
average
Absorption coefficient (Mm-1) at 532nm
Local time (hr)

a)

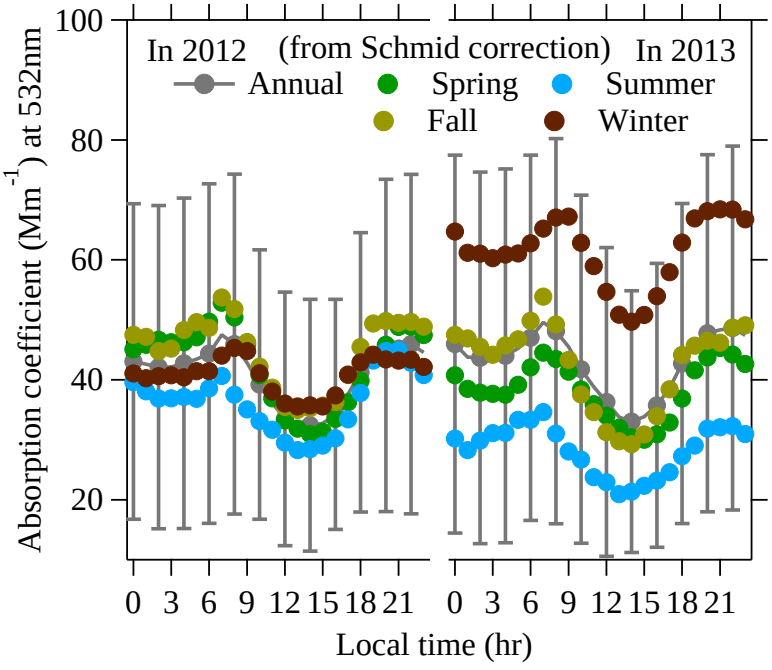
In 2012
(from Schmid correction)
In 2013
Annual
Spring
Summer
Fall
Winter
Absorption coefficient (Mm-1) at 532nm
Local time (hr)

b)

Figure 4

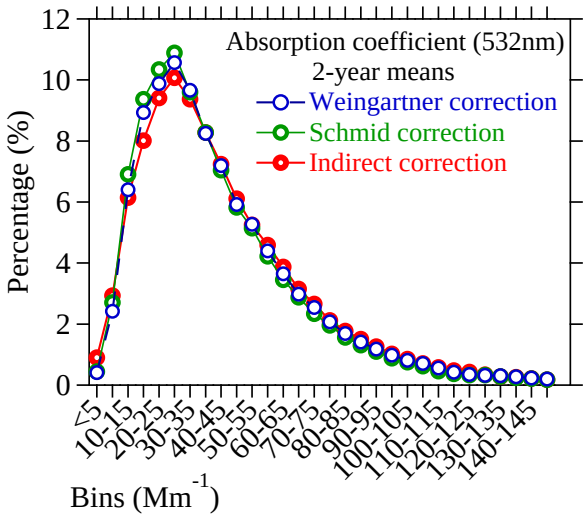
Absorption coefficient (532nm)
2-year means
Weingartner correction
Schmid correction
Indirect correction
Percentage (%)
Bins (Mm-1)

a)

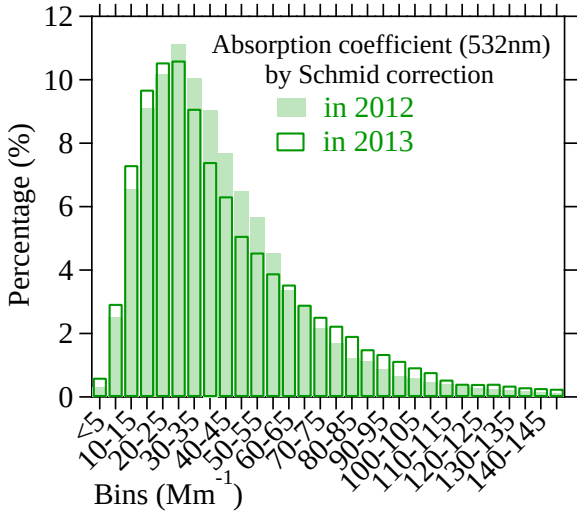
Absorption coefficient (532nm)
by Schmid correction
in 2012
in 2013
Percentage (%)
Bins (Mm-1)

b)

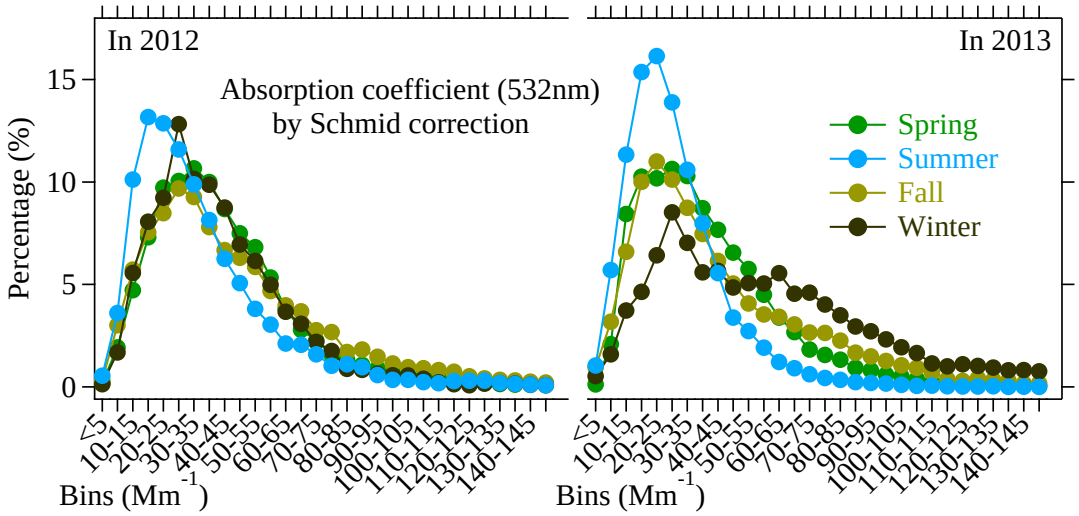
In 2012
In 2013
Absorption coefficient (532nm)
by Schmid correction
Spring
Summer
Fall
Winter
Percentage (%)
Bins (Mm-1)

c)

Figure 5

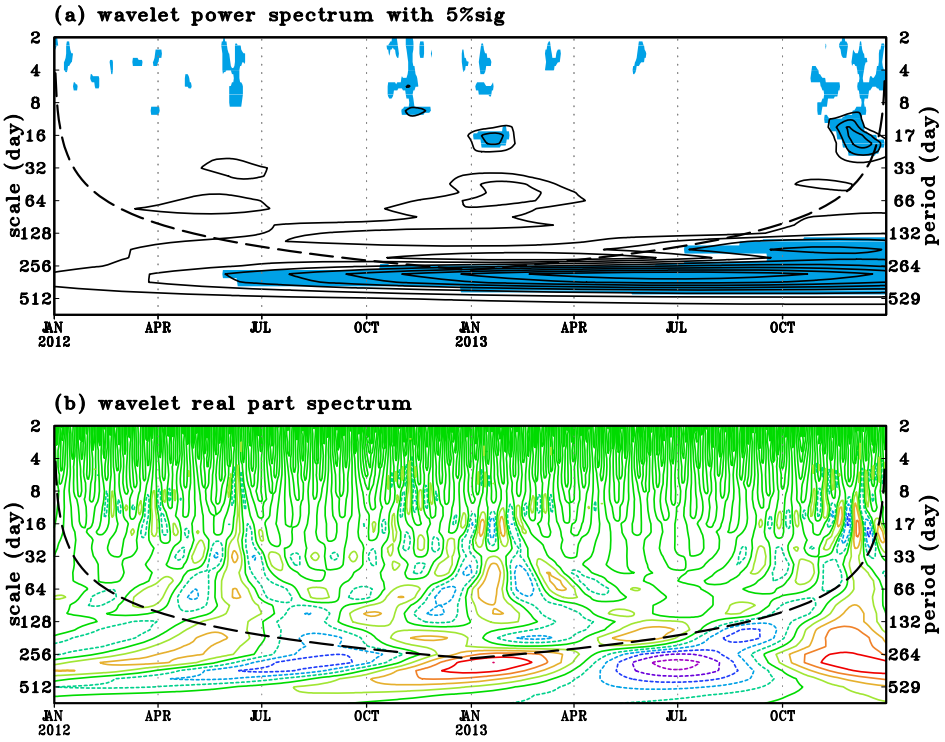
(a) wavelet power spectrum with 5%sig
scale (day)
period (day)
2
4
8
16
32
64
128
256
512
17
33
66
132
264
529
JAN
2012
APR
JUL
OCT
JAN
2013
APR
JUL
OCT
(b) wavelet real part spectrum
scale (day)
period (day)
JAN
2012
APR
JUL
OCT
JAN
2013
APR
JUL
OCT

Figure 6

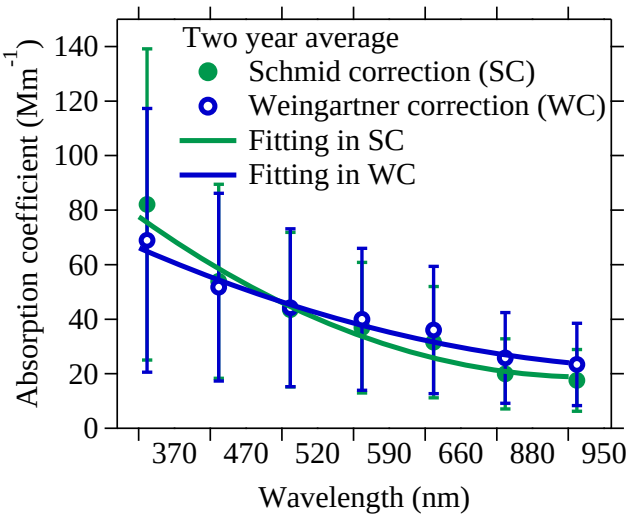

745

746 a)

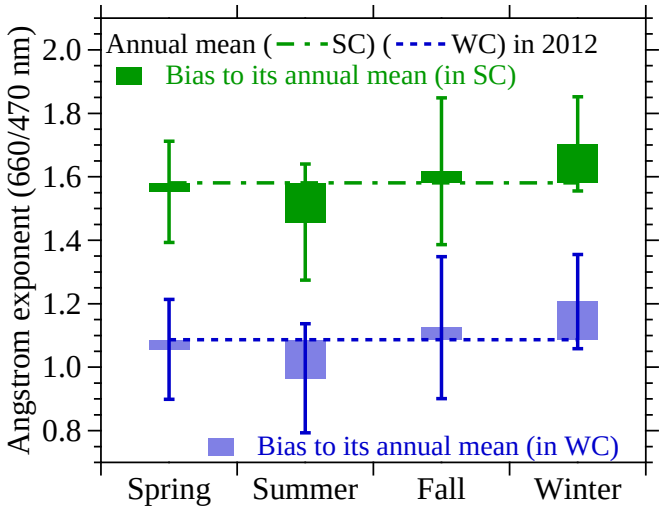

747

748 b)

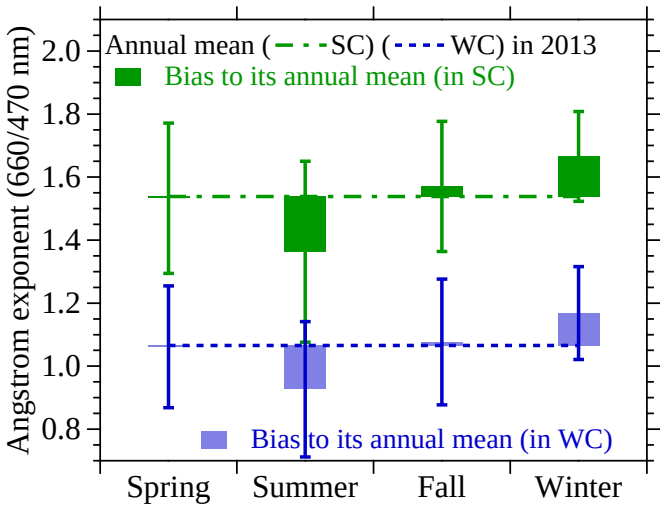

749

750 c)

751 Figure 7

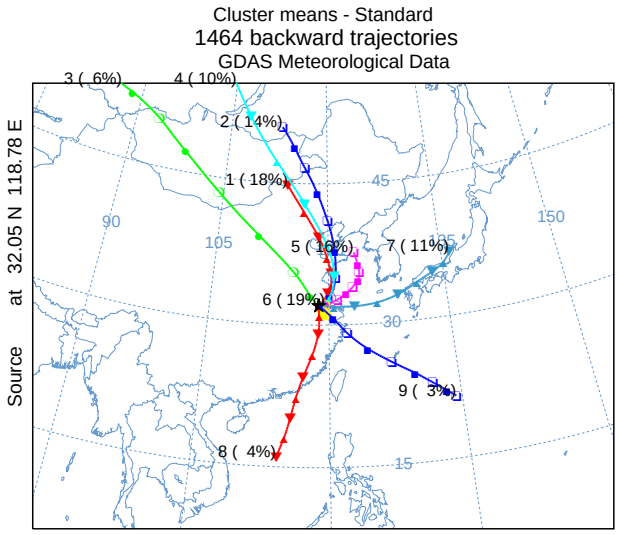
Cluster means - Standard
1464 backward trajectories
GDAS Meteorological Data
Source at 32.05 N 118.78 E
3 (6%)
4 (10%)
2 (14%)
1 (18%)
5 (16%)
7 (11%)
6 (19%)
9 (3%)
8 (4%)
45
90
105
135
150
30
15

a)

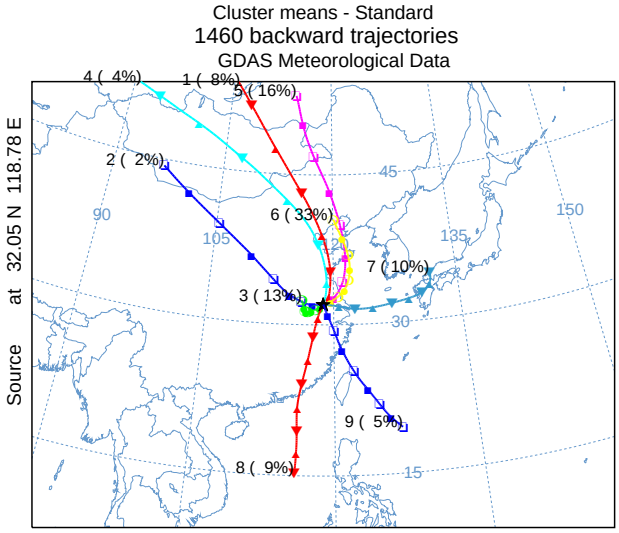
Cluster means - Standard
1460 backward trajectories
GDAS Meteorological Data
Source at 32.05 N 118.78 E
4 (4%)
1 (8%)
5 (16%)
2 (2%)
6 (33%)
7 (10%)
3 (13%)
9 (5%)
8 (9%)
45
90
105
135
150
30
15

b)

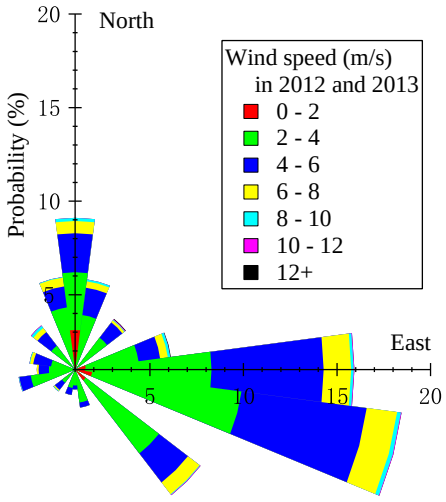
North
East
Probability (%)
20
15
10
5
10
15
20
Wind speed (m/s)
in 2012 and 2013
0 - 2
2 - 4
4 - 6
6 - 8
8 - 10
10 - 12
12+

c)

Figure 8

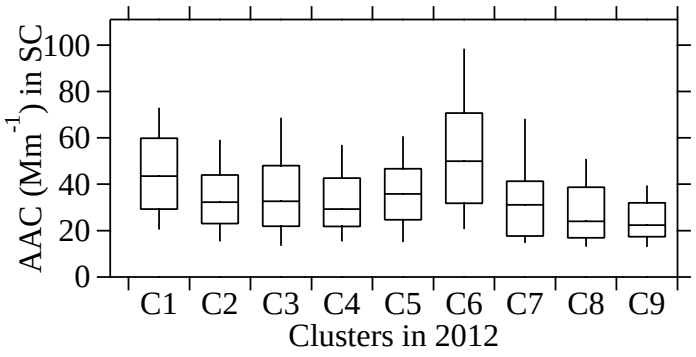

759

760 a)

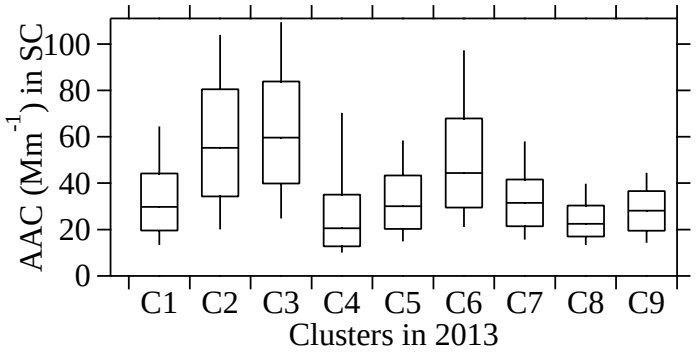

761

762 b)

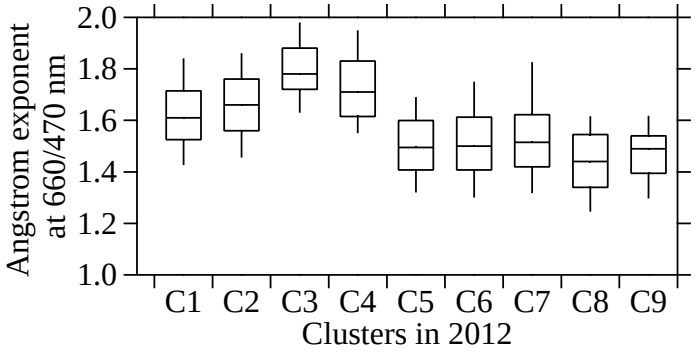

763

764 c)

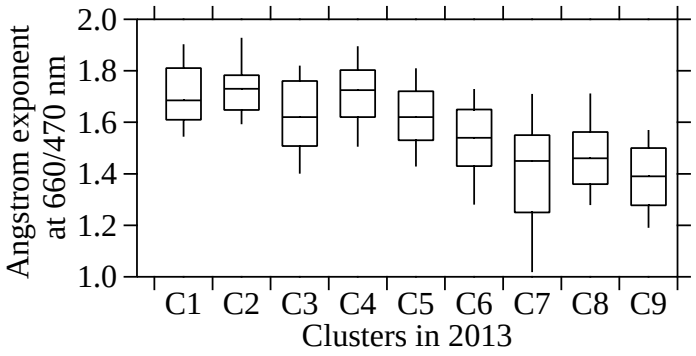

765

766 d)

767 Figure 9

768

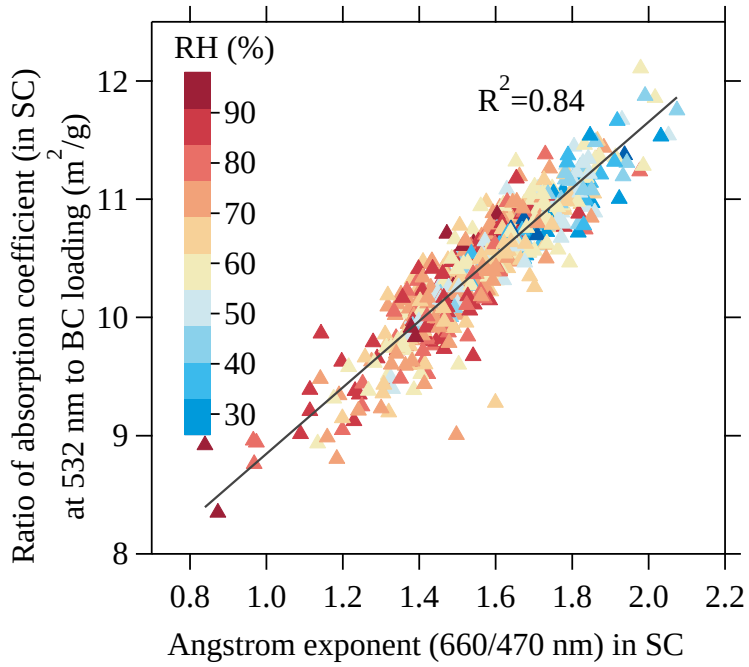
RH (%)
90
80
70
60
50
40
30
R2=0.84
Ratio of absorption coefficient (in SC) at 532 nm to BC loading (m2/g)
Angstrom exponent (660/470 nm) in SC
8
9
10
11
12
0.8
1.0
1.2
1.4
1.6
1.8
2.0
2.2

a)

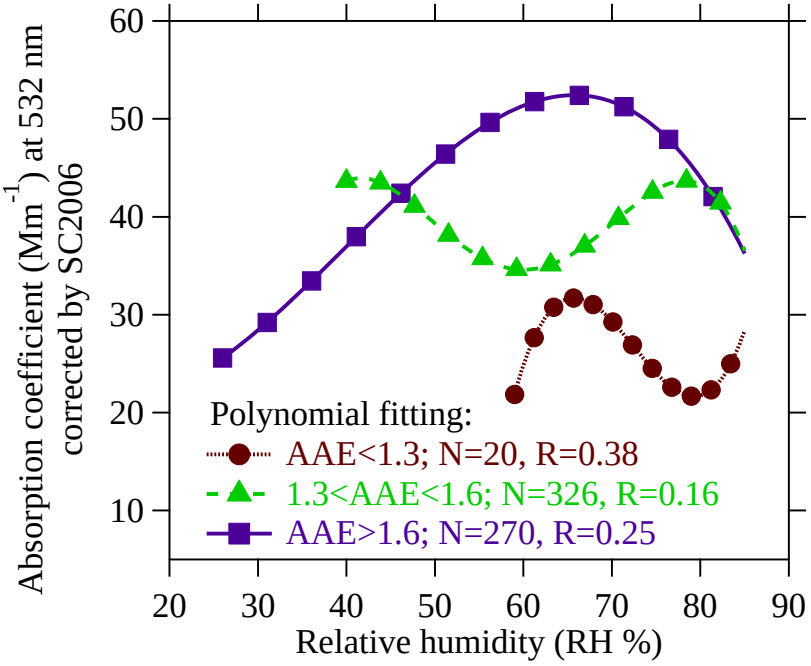
Absorption coefficient (Mm-1) at 532 nm corrected by SC2006
Relative humidity (RH %)
Polynomial fitting:
AAE<1.3; N=20, R=0.38
1.3<AAE<1.6; N=326, R=0.16
AAE>1.6; N=270, R=0.25
10
20
30
40
50
60
20
30
40
50
60
70
80
90

b)

Figure 10

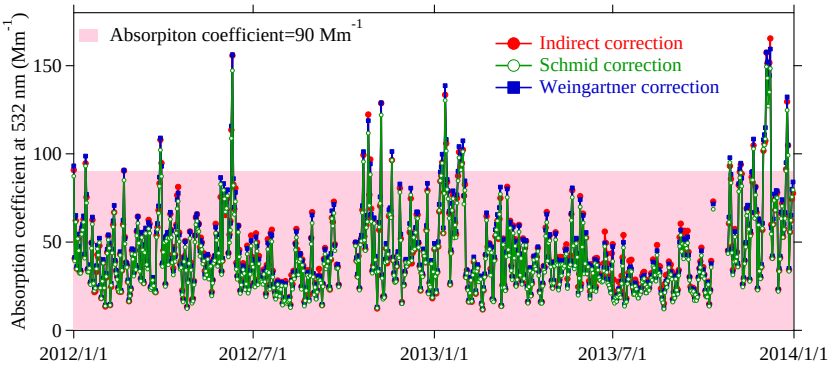

778

779 Figure 11

780

781